

# A Model for Targeting Colon Carcinoma Cells Using Single-Chain Variable Fragments Anchored on Virus-Like Particles via Glycosyl Phosphatidylinositol Anchor

メタデータ	言語: eng 出版者: 公開日: 2015-03-02 キーワード (Ja): キーワード (En): 作成者: Deo, Vipin Kumar, Yui, Megumi, Alam, Md. Jahangir, Yamazaki, Masahito, Kato, Tatsuya, Park, Enoch Y. メールアドレス: 所属:
URL	<a href="http://hdl.handle.net/10297/8100">http://hdl.handle.net/10297/8100</a>

# **A Model for Targeting Colon Carcinoma Cells using Single-chain Variable Fragments Anchored on Virus-like Particles via Glycosyl Phosphatidylinositol Anchor**

Vipin Kumar Deo • Megumi Yui • Md. Jahangir Alam • Masahito Yamazaki •  
Tatsuya Kato • Enoch Y Park\*

Running Head: Cell targeting using scFvs anchored on VLPs via GPI anchor

---

V. K. Deo • Tatsuya Kato • Enoch Y. Park (✉)  
Research Institute of Green Science and Technology, Shizuoka University, 836 Ohya,  
Suruga-ku, Shizuoka 422-8529, Japan  
Tel.: +81 54 238 4887; fax: +81 54 238 4887. e-mail: [acypark@ipc.shizuoka.ac.jp](mailto:acypark@ipc.shizuoka.ac.jp)

Megumi Yui • Tatsuya Kato • Enoch Y. Park  
Laboratory of Biotechnology, Department of Applied Biological Chemistry, Faculty of  
Agriculture, Shizuoka University, 836 Ohya, Shizuoka 422-8529, Japan

Masahito Yamazaki • Enoch Y. Park  
Graduate School of Science and Technology, Shizuoka University, 836 Ohya, Shizuoka 422-  
8529, Japan

Masahito Yamazaki • Jahangir Mohammed Alam  
Research Institute of Electronics, Shizuoka University, 836 Ohya, Suruga-ku, Shizuoka 422-  
8529, Japan

1 **ABSTRACT**

2 **Purpose** VLPs displaying tumor targeting single-chain variable fragments  
3 (VLP-rscFvs) which targets tumor-associated glycoprotein-72 (TAG-72)  
4 marker protein have a potential for immunotherapy against colon carcinoma  
5 tumors. In this study, scFvs anchored on VLPs using  
6 glycosylphosphatidylinositol (GPI) were prepared to target colon carcinoma  
7 spheroids in vitro.

8 **Methods** VLPs-rscFvs were produced by co-injecting two types of *Bombyx*  
9 *mori* nucleopolyhedrovirus (BmNPV) bacmids, encoding RSV-gag and rscFvs  
10 cDNA into silkworm larvae. Large unilamellar vesicles (LUVs) of 100 nm in  
11 diameter were made using 1,2-dioleoyl-*sn*-glycero-3-phosphocholine (DOPC)  
12 and packaged with Sulforhodamine B (SRB). LUV-SRB was used to associate  
13 with VLP-rscFvs assisted by GP64 present on VLP-rscFvs to produce VLP-  
14 rscFv associated SRB (VLP-rscFvs-SRB) at pH 7.5.

15 **Results** The antigenicity of the purified VLPs-rScFvs was confirmed by  
16 enzyme-linked immunosorbent assay (ELISA) using TAG-72 as antigen. LUV-  
17 SRB made of DOPC was used to associate with 100 µg of VLP-rscFvs to  
18 produce VLP-rscFv-SRB. Specific delivery and penetration of SRB up to 100  
19 µm into the spheroids shows the potential of the new model.

20 **Conclusions** The current study demonstrated the display, expression and  
21 purification of VLP-rscFvs efficiently. As a test model VLP-rscFv-SRB were  
22 prepared which can be used for immunotherapy. rscFvs provide the specificity  
23 needed to target tumors and VLPs serve as carrier transporting the dye to  
24 target.

25 **KEYWORDS** single-chain variable fragment • virus-like particle • silkworm  
26 expression system • tumor-associated glycoprotein-72 • large unilamellar  
27 vesicle

## 28 **ABBREVIATIONS**

29 CLSM                    confocal laser scanning microscope  
30 DOPC                    1,2-dioleoyl-*sn*-glycero-3-phosphocholine  
31 BmNPV                    *Bombyx mori* nucleopolyhedrovirus  
32 ELISA                    enzyme-linked immunosorbent assay  
33 gag                        group antigen protein  
34 GPI                        glycosylphosphatidylinositol  
35 mAbs                    monoclonal antibodies  
36 LUVs                    large unilamellar vesicles  
37 RSV                        *Rous sarcoma* virus  
38 scFvs                    single-chain variable fragments  
39 SRB                        Sulforhodamine B  
40 TAG-72                    tumor associated glycoparticle-72  
41 VLPs                    virus-like particles  
42 VLP-rscFvs                VLPs displaying tumor targeting scFVs  
43 VLP-rscFv-SRB            VLP-rscFv packaged SRB

44

## 45 INTRODUCTION

46 Virus like particles (VLPs) are macromolecular structures that are formed using  
47 capsid protein from virus which can self-fold to form VLPs and are incapable of  
48 infection because they are devoid of genetic material. Group antigen protein (gag)  
49 protein from *Rous sarcoma* virus (RSV) species belonging to the family *Retroviridae*,  
50 subfamily *Orthoretrovirinae*, genus *Alpharetrovirus* of single stranded RNA virus  
51 forms VLPs. gag protein used in the present study is composed of 577 amino acid  
52 length with 61 kDa molecular weight, devoid of the protease region (1). It is  
53 composed of a membrane-binding domain that directs the gag protein to the plasma  
54 membrane via a well-known lipid raft pathway conserved in retrovirus family (2, 3).  
55 The interaction domain promotes gag-gag multimerization important for particle  
56 assembly to form the VLPs of approximately 80–100 nm and the late assembly  
57 domain later facilitates the pinching of viral particles enveloped in a lipid layer from  
58 the plasma membrane assisted by proteases (2, 4). Lipid layer can be used to display  
59 membrane bound proteins on VLPs surface using glycosylphosphatidylinositol (GPI)  
60 anchor domain of proteins (5). The GPI moieties are widely spread in living  
61 organisms, playing significant role in providing varying biological functions (6). GPI-  
62 anchoring of the proteins takes place in the endoplasmic reticulum membrane at  
63 specific site recognized by enzymes enabling the protein to hitch a ride on lipid rafts  
64 and reach plasma membrane undergoing the post-translational changes (7, 8). A  
65 simple but efficient process, the C-termini of protein covalently attached to GPI via  
66 fatty acid chain is stably associated with the membrane. Use of GPI anchored proteins  
67 is well-known for detection as well as for targeting disease-causing factors for therapy  
68 (9–11). GPI anchored antibodies on VLPs have not yet been studied but antibodies

69 fused with GPI anchored in lipid membranes has been shown to be useful and  
70 effective against targets such as HIV-1 envelope spikes for neutralization (12).

71 Immunotherapy has been revolutionized by the successful screening and  
72 development of numbers of monoclonal antibodies (mAbs) against specific markers  
73 on cancer as a tool for therapy (13, 14). CC49 is a clinically validated antibody to  
74 target a tumor-associated glycoprotein-72 (TAG-72) a well-known marker in colon  
75 carcinoma (15). mAbs coupled with or without toxins or chemical drugs have been  
76 marketed under different names like anatumomab, mafenatox and minretumomab as  
77 chemo-therapy treatment an alternative to surgical treatment method (16). mAbs  
78 conjugated to drugs or by themselves when administered in patients to target tumors  
79 have less penetration and only 20% of the administered dose interacts with the tumors  
80 (17). mAbs also show clinical bottleneck of aggregation in kidney and other organs  
81 involved in removal of toxic materials due to extended biological half-life (2–3 weeks  
82 depending on class of antibody) in blood circulatory system (13, 17). Alternatively,  
83 single-chain variable fragment (scFvs) linked by a short linker has shown high  
84 specificity and relatively low biological half-life (less than 2 h) allowing it to be used  
85 as a radio labeled molecule for imaging and diagnosing tumors in patients. Shorter  
86 retention time is also one of the main downfalls as the duration its available in the  
87 circulatory system is not enough for drug delivery. Different drug delivery systems  
88 using scFvs conjugated to drugs or fused with other proteins to be activated on site of  
89 target, increase its retention time and enhance the delivery of drug to tumor (15, 18).  
90 The biggest disadvantage of such an approach is that modifying the protein by  
91 chemical process to tag the scFvs with drugs or enzyme fused with scFvs causes  
92 improper folding and loss of scFvs function (19). Hence here a novel approach of

93 displaying recombinant scFvs (rscFvs) anchored with GPI embedded in the lipid layer  
94 of VLPs is studied.

95         The silkworm expression system uses silkworm larvae to express and purify  
96 proteins efficiently at milligrams level, using *Bombyx mori* nucleopolyhedrovirus  
97 (BmNPV), which belongs to the double-stranded DNA virus family *Baculoviridae* (1).  
98 BmNPV infects silkworms using spike proteins on baculovirus envelope, like  
99 glycoprotein 64 (GP64) a type I membrane protein to associate and fuse with cell  
100 membrane to infect silkworms (20–22). GP64 is further classified as type III  
101 membrane fusion protein class depending upon its fusion property of initiating fusion  
102 independently without any help by forming large fusion pores rapidly. Association of  
103 GP64 with membranes takes place first leading to fusion of GP64 to lipid membrane  
104 driven by protonation of Histidine amino acids ( $pK_a$  6.0) (23, 24). Previously, it has  
105 been reported that RSV gag VLPs expressed and purified using baculovirus  
106 expression system have GP64 peppered on its surface (25). Here the use of functional  
107 GP64 on VLPs and their association with large unilamellar vesicles (LUVs)  
108 membrane in developing a new drug delivery system is studied. The focus is on  
109 developing VLPs-rscFvs as a model drug delivery system associated with hydrophilic  
110 fluorescent dyes by LUVs. LUVs only packaged with either hydrophilic or  
111 hydrophobic fluorescent dyes are well known for studying drug delivery to 3D tumors  
112 spheroid model (26–28). The ex vivo 3D spheroid models offer a platform to study  
113 and gain insight into drug delivery properties of rapidly evolving new drug delivery  
114 tools. The major drawback of using LUVs alone packaged with drugs as a tool for  
115 therapy is the non-specificity and the toxicity resulting due to accumulation in  
116 detoxification related organs and tissue in humans. LUVs with various marker  
117 proteins or baculovirus fused with LUVs have been studied as a drug delivery tool (24,

118 29). Such an approach has either high toxicity or due to use of large baculovirus  
119 which carries genetic material causes health and infection concerns and its use is  
120 curtailed. Hence the current study focus is on developing a new model system devoid  
121 of any genetic material with high target specificity provided by rscFvs anchored on  
122 VLPs by GPI carrying a test fluorescent dye.

123 In the current study, feasibility of using VLPs a macromolecular structure  
124 displaying rscFvs targeting cancer cells and spheroids made from the same cells has  
125 been tested. The current approach uses GPI to anchor scFv on VLPs without putting  
126 any protein folding constraints on either scFv-GPI or gag-gag multimerization for  
127 VLPs formation. In addition, LUVs packaged with sulforhodamine B (SRB) a water-  
128 soluble fluorescent dyes to associate with VLPs displaying rscFv and GP64 as a  
129 model to test an effective drug delivery. SRB a water soluble negatively charged  
130 aminoxanthine dye is used for cell based cytotoxicity assay in various cancer cell  
131 lines with better accuracy than other known assay (30). Utilizing GP64 is important  
132 for large-scale application because VLPs displaying rscFvs can be made with ease by  
133 the silkworm expression system and the VLPs can serve as carrier of drugs or dyes to  
134 give the extra merit needed in rapidly evolving drug delivery systems targeting  
135 tumors.

## 136 **MATERIALS AND METHODS**

### 137 Cell lines and Media

138 LS174T human colon adenocarcinoma cell line (ATCC CL-188) was obtained from  
139 ATCC (Manassas, VA, USA) and HEK293 (RCB1637) was obtained from Riken Bio  
140 Resource Center (Tsukuba-shi, Ibaraki, Japan). **LS174T presenting a tumor associated**  
141 **glycoprotein-72 (TAG-72) on cell surface, was cultured in 60 mm culture plates** (TPP,

142 Trasadingen, Switzerland) with MEM-eagle medium (Sigma-Aldrich, St. Louis, MO,  
143 USA) containing 10% (v/v) fetal bovine serum (Invitrogen, Carlsbad, CA, USA),  
144 supplemented with 1% (v/v) antibiotic solution containing penicillin, streptomycin,  
145 fungizone (Sigma-Aldrich) and incubated at 37°C in 5% CO<sub>2</sub> incubator (MCO-175  
146 Sanyo, Osaka, Japan). HEK293 were cultured in 60 mm culture plates with  
147 MEM/EBSS (HyClone Laboratories Inc., Utah, USA) containing 2 mM L-glutamine,  
148 1% non-essential amino acid (Invitrogen), 10% fetal bovine serum, supplemented  
149 with 1% (v/v) antibiotic solution containing penicillin, streptomycin, fungizone and  
150 incubated at 37°C in 5% CO<sub>2</sub> incubator. Both the cell lines were grown till confluence  
151 and splitting was done in 1 : 5 ratio once every week by trypsinisation using TrypLE  
152 Express (Life Technologies Japan LTD., Minato-Ku, Tokyo, Japan) for 15 minutes at  
153 37°C in 5% CO<sub>2</sub> incubator.

#### 154 PCR Amplification and Bacmid Preparation

155 Using PredGPI software the GPI anchor position and the nucleotide sequence was  
156 confirmed as previously reported for VLPs displaying rNcSRS2 (31) and the same  
157 GPI anchor is used in current work. The plasmid carrying CC49 gene was kindly  
158 provided by Professor Hiroshi Ueda (Tokyo Institute of Technology, Japan). The scFv  
159 cDNA was cloned by PCR into pENTR to make pENTR/scFv-DDDDK. The GPI  
160 anchor cDNA was inserted in frame by PCR using pENTR/scFv-DDDDK plasmid as  
161 template using forward primer 5'-  
162 caccatgaagataactccttgctattgcattaatggtgtcaacagtaatgtgggtgtcaacagactacaaggatgacgat  
163 gacaag-3' and reverse primer 5'-  
164 ttatcagtacgcaaagattgccgttcagtcagtgacgcagcggatagtgccacgtacgaaggcaactcgtcacatgcatc  
165 tccgatccccccccggttaa-3' respectively. The forward primer contained 63 base pair

166 Bombyxin signal (bold) sequence followed by DDDDK affinity tag nucleotide  
167 sequence (dashed line). The reverse primer contained the 81 base pair of putative GPI  
168 signal (underlined) motif of NcSRS2. PCR products were inserted into the entry  
169 vector, pENTR/D-TOPO (Invitrogen) to give pENTR/scFv-GPI. The PCR fragment  
170 inserted into pENTR/D-TOPO was confirmed by dideoxynucleotide chain  
171 terminating sequence (32) using Thermo Sequenase Cycle Sequencing kit (USB Co.,  
172 Cleveland, Ohio, USA). pENTR/scFv-GPI was used to transfer scFv-GPI to pDEST8  
173 by LR reaction according to the protocol to make pDEST8/scFv-GPI, which was used  
174 to transform to *E. coli* BmDH10bac competent cells to make recombinant bacmids  
175 (33). White colonies of recombinant bacmid carrying scFv-GPI gene were isolated  
176 and resulting bacmid was designated as BmNPV bacmid/VLP-rscFvs.

177 Bacmid/RSV-gag-577 from previously reported work is used (1) and the  
178 BmNPV bacmids were isolated and resuspended in phosphate buffered saline  
179 containing 80 mM di-sodium hydrogen orthophosphate anhydrous, 19 mM sodium di-  
180 hydrogen orthophosphate anhydrous, and 100 mM sodium chloride (PBS, pH 7.5) for  
181 injection.

## 182 Silkworm Larvae Rearing, Feeding and Injection

183 Fifth instars larvae (Ehime Sansyu Co. Ltd., Ehime, Japan) were reared on an  
184 artificial diet Silkmate S2 (Nihon Nosan Kogyo, Yokohama, Japan) in a 65%  
185 humidity chamber (MLR-351H, Sanyo, Tokyo, Japan) at 27°C.

186 Each silkworm was injected with 40 µL recombinant bacmid DNA solutions  
187 containing 10 µg of BmNPV-gag577 and BmNPV-scFv-GPI bacmids, respectively, in  
188 10% (v/v) DMREI-C reagent (Invitrogen) in PBS using 1 mL syringe. Post injection  
189 7<sup>th</sup> day the silkworm larval hemolymph was harvested in tubes (Falcon, Lincoln Park,

190 NJ, USA) containing 2 mM phenyl thiourea and complete EDTA-free protease  
191 inhibitor cocktail to inhibit the hemolymph melanization and protein degradation by  
192 proteases. These samples were aliquoted into eppendorf tubes and stored at -80°C.

### 193 Purification of VLPs Displaying scFvs-GPI

194 VLP-rscFvs containing hemolymph collected from silkworm larvae were centrifuged  
195 at 1,000 g in a Heraeus Primo R Sorvall Biofuge (Thermo Scientific, Yokohama,  
196 Japan) for 3 min using Heraeus 7591 swing bucket rotor to remove debris. The clear  
197 hemolymph was dialyzed with cellulose ester dialysis membrane (Spectrum  
198 Laboratories Inc., California, USA) having 300,000 molecular weight cut off in 2 L of  
199 PBS (pH 7.5) for overnight at 4°C. The dialyzed hemolymph was centrifuged at  
200 14,010 g using micro refrigerated centrifuge (Model 3700, Kubota, Tokyo, Japan) for  
201 10 min at 4°C to remove any aggregates and the supernatant was filter-sterilized with  
202 5 µm filter membrane (Merck-Millipore, MA, USA). The protein sample was added  
203 to PBS pre-equilibrated 5 mL of DDDDK-agarose gel (Medical and Biological  
204 Laboratories Co., Ltd., Nagoya, Japan) in batch mode and purification performed as  
205 per the kit protocol. Elution was carried out using 0.1 mg/mL DDDDK peptide  
206 (Medical & Biological Laboratories Co., Ltd., Nagoya, Japan) in 500 µL aliquots. The  
207 protein concentrations were measured using standard BCA protein estimation kit  
208 (Pierce BCA Assay kit, IL, USA).

### 209 Western-blot Analysis

210 To detect the expression of VLPs and rscFvs, larval hemolymph from silkworm  
211 larvae were collected. Samples were subjected to 10% (w/v) SDS-PAGE using the  
212 mini-protean II system (Bio-Rad, Hercules, California, USA). After SDS-PAGE,

213 proteins were blotted on to a PVDF membrane using the Mini Trans-Blot  
214 Electrophoretic Transfer cell (Bio-Rad) at 15 V for 1 h. The membranes were probed  
215 with 5,000 and 2,000 fold diluted mouse anti-DDDDK primary antibodies (Wako  
216 Pure Chem. Ind. Ltd., Osaka, Japan) for rscFvs and rabbit anti-RSV-gag primary  
217 antibody for gag-577 (1), respectively, in Tris-buffered saline with 0.1% (v/v) Tween-  
218 20 (TBS-T) (Wako) for 1 h at room temperature with mild shaking. Secondary  
219 antibodies conjugated with horseradish peroxidase (HRP) were goat anti-mouse IgG  
220 (Santa Cruz Biotechnology, Santa Cruz, CA, USA) for rscFvs and goat anti-rabbit  
221 IgG (Santa Cruz Biotechnology) for gag-577, respectively. The secondary antibodies  
222 were incubated for 1 h at room temperature and specific bands for rscFvs and gag-577  
223 proteins were detected using an Immobilon western blotting reagent pack (Millipore  
224 Corporation, Billerica, Massachusetts, USA). The rscFvs and gag-577 proteins bands  
225 were analyzed using a Fluor-S/MAX multi-imager (Bio-Rad).

#### 226 Confirmation of the Antigen Specificity of rscFvs Displayed on VLPs by ELISA

227 Human TAG-72 at 20 U per well (Sigma-Aldrich) in 100  $\mu$ L volume was  
228 immobilized in an immuno plate (Thermo Scientific, West Palm Beach, FL, USA),  
229 overnight at 4°C in triplicates. The plates were blocked with 100  $\mu$ L/well Ez-block  
230 Chemi (ATTO Co., Tokyo, Japan) for 1 h at room temperature and washed thrice with  
231 200  $\mu$ L/well PBS (pH 7.5). Five micrograms of VLP-rscFvs and VLPs were added to  
232 each well, respectively and incubated for 2 h at room temperature. After incubation,  
233 the plates were washed three times with 200  $\mu$ L/well PBS (pH 7.5). The plates were  
234 incubated with 100  $\mu$ L/well mouse anti-DDDDK antibody 2,000 fold diluted in PBS-  
235 T (Tween-20 0.1% (v/v)) and incubated for 1 h at room temperature. After incubation  
236 the plates were washed thrice with 200  $\mu$ L/well PBS-T pH 7.5 and incubated with

237 goat anti-mouse IgG conjugated with HRP 4,000 fold diluted in PBS-T for 1 h at  
238 room temperature. After incubation the plates were washed thrice with 200  $\mu$ L/well  
239 PBS-T (pH 7.5) and detection was carried out using 3,3',-5,5'-tetramethylbenzidine  
240 (TMBZ) (Dojindo, Kumamoto, Japan) solutions by observing the absorbance at 450  
241 nm by Plate reader (Bio-Rad) (5).

#### 242 Phospholipase C Treatment of VLP-scFv-GPI

243 Each well of immuno plate was immobilized with 5  $\mu$ g of VLP-rscFvs and VLPs,  
244 respectively for overnight at 4°C in triplicates. The plates were blocked and treated  
245 with primary and secondary antibodies similar to ELISA method. After incubation the  
246 plates were washed three times with 200  $\mu$ L/well PBS-T (pH 7.5) and presence of the  
247 GPI anchor from the lipid layer was confirmed by digestion with 0.1 U of  
248 phosphatidyl-inositol specific Phospholipase C (PI-PLC) (Sigma-Aldrich) in 200  
249  $\mu$ L/well PBS (pH 7.5) for 2 h at 27°C. After incubation the plates were washed and  
250 scFv was detected similar to ELISA method.

#### 251 Hemolysis Assay

252 Rabbit erythrocytes (Nihon BioTest Research, Tokyo, Japan) were prepared and 2.5%  
253 (v/v) were seeded per 96-well plate in triplicates (34). Purified VLP-rscFvs and  
254 Bovine serum albumin (100  $\mu$ g/mL) as a negative control were added and allowed to  
255 absorb for 10 min on ice. Then, the mixture was incubated for 30 min at 37°C. Extent  
256 of hemolysis was determined spectrophotometrically at 540 nm in a plate reader (Bio-  
257 Rad).

#### 258 Liposome Preparation and Sulforhodamine B Packaging

259 Multilamellar vesicles (MLVs) were prepared using 10 mM 1,2-dioleoyl-*sn*-glycero-  
260 3-phosphocholine (DOPC) (Avanti Polar Lipids, Alabaster, Alabama, USA) dissolved  
261 in chloroform (Wako) in 5 mL glass vial with a cap. DOPC was evaporated under  
262 flowing nitrogen gas, films formed at the bottom of the vial and were kept in a  
263 desiccator in vacuum overnight for complete drying of chloroform. Films were then  
264 hydrated by adding PBS (pH 7.5) containing 1 mM sulforhodamine 101 acid chloride  
265 (SRB) (Dojindo, Kumamoto, Japan) at room temperature by vortexing five times for  
266 20 seconds. SRB was packaged into MLVs by freeze thawing method in a three-step  
267 cycle of 20 min. MLVs were extruded using Avanti Mini-extruder (Avanti Polar  
268 Lipids) with a 19 mm diameter polycarbonate 100 nm pore size membrane (Avestin,  
269 Ontario, Canada) 20 times to produce LUVs packaged with SRB (LUV-SRB). LUV-  
270 SRB mixture containing LUVs and LUVs-SRB were resolved on pre-equilibrated  
271 sephadex G75 (7 cm × 3 cm dimensions) column (Terumo, Tokyo, Japan). The  
272 purified LUV-SRB suspension was collected from the void volume fraction and  
273 concentration of the lipid and SRB were estimated (35). Lipid estimation was done by  
274 Fiske-Subbarow colorimetric method using LUV-SRB prepared in HEPES buffer pH  
275 7.5 under conditions similar as described above. The SRB excitation and emission  
276 measurements were taken at 515 and 604 nm, respectively by a 96 well  
277 spectrophotometer (Tecan Japan Co., Ltd., Kawasaki, Japan).

278 One hundred micrograms of VLP-rscFvs in 500  $\mu$ L of PBS (pH7.5) buffer  
279 were mixed with 500  $\mu$ L of LUV-SRB containing 28.8  $\mu$ M DOPC and 1 mM SRB.  
280 The mixture VLP-rscFv-LUV-SRB (VLP-rscFv-SRB) was incubated for 1 h at 27°C  
281 for association to be complete. Small aliquot from VLP-rscFv-SRB sample was used  
282 for SRB concentration measurement.

283 Dynamic Light Scanning (DLS) Measurement

284 One hundred micrograms of purified VLP-rscFvs and VLP-rscFv-SRB were extruded  
285 using Avanti Mini-extruder (Avanti Polar Lipids) with a 19 mm diameter  
286 polycarbonate 200 nm pore size membrane (Whatman Japan Ltd., Tokyo, Japan)  
287 three times to get uniformly dispersed sample. The samples were loaded in disposable  
288 cuvettes (DTS-1061) for measurement of size with the Zetasizer Nano series  
289 (Malvern, Worcestershire, United Kingdom).

## 290 Transmission Electron Microscopy (TEM) of VLP-scFvs-GPI and its 291 Packaging

292 The purified VLPs-rscFvs, LUV-SRB and VLP-rscFv-SRB samples respectively were  
293 spotted on carbon grids (Okenshoji, Tokyo, Japan) and dried at room temperature.  
294 Negative staining was performed using 2% (v/v) phosphotungstic acid (Wako) as  
295 described previously (5). For immunoelectron microscopy, VLPs-rscFvs and VLP-  
296 rscFv-SRB samples were loaded on the grids in similar fashion and the grids were  
297 blocked using 4% (w/v) bovine serum albumin (BSA) (Sigma-Aldrich) for 1 h and  
298 washed with PBS (pH 7.5). The grids were incubated in PBS containing mouse anti-  
299 DDDDK at 1:100 dilutions for 2 h, and washed with PBS. Subsequently, the grids  
300 were incubated in PBS containing 1:200 diluted goat anti-mouse IgG conjugated with  
301 10 nm gold particles (BB International, Cardiff, UK) for 2 h, and washed with PBS.  
302 Negative staining was performed as mentioned above and samples were observed at  
303 50,000 × magnification (JEM 2100F-TEM, JEOL Ltd., Akishima, Tokyo, Japan)  
304 operating at 200 kV. The high-resolution TEM images were transformed using fast  
305 Fourier transformation function available with the instrument.

## 306 Confirming Specificity of VLP-rscFvs

307 LS174T and HEK293 cell lines were cultured for 3 days and around  $10^4$  cells were  
308 seeded on glass slides (2.6 cm  $\times$  7.6 cm) (Matsunami Glass Ind., LTD., Osaka, Japan)  
309 and incubated overnight under growing conditions. The cells were washed  
310 respectively with fresh medium and incubated with 3  $\mu$ g of VLP-rscFvs for 3 h. The  
311 cells respectively were treated with 500 fold diluted BODIPY FL-C5-ceramide  
312 conjugated to BSA (Invitrogen) and mouse monoclonal anti-DDDDK-tag-Alexa  
313 Fluor 594 (MBL Co. LTD., Nagoya, Aichi, Japan) respectively and incubated for 1 h  
314 at 37°C. The cells were then washed with fresh growth medium and incubated with  
315 1,000 fold diluted 4'-6-Diamidino-2-2-Phenylindole, Hydrochloride (DAPI) solution  
316 for 1 h at 37°C. The cells were washed once respectively, fixed using 2% (v/v)  
317 formaldehyde and viewed under confocal laser scanning microscope (CLSM) (LSM  
318 700, Carl Zeiss, Oberkochen, Germany) with Plan-apochromat 40  $\times$  (2.5 zoom factor)  
319 oil lens respectively. Zen LE software available on Carl Zeiss website was used for  
320 image analysis.

321 Similar amount of VLP-rscFvs as used above was also fixed on glass slides  
322 and treated with 500 fold diluted mouse monoclonal anti-DDDDK-tag-Alexa Fluor  
323 594 and incubated for 1 h at 37°C. VLP-rscFvs samples were not stained with DAPI  
324 as there was no nucleus present. The samples were fixed as mentioned above and  
325 observed under CLSM with Plan-apochromat 100  $\times$  (1 zoom factor) oil lens. Zen LE  
326 software available on Carl Zeiss website was used for image analysis.

### 327 Delivery of VLP-rscFv-SRB

328 LS174T cells as mentioned above were cultured and seeded on the slides. The cells  
329 were washed with fresh medium and incubated with 3  $\mu$ g of VLP-rscFv-SRB and 100  
330  $\mu$ L of LUV-SRB as a negative control for 3 h. The cells were washed and treated with

331 500 fold diluted mouse monoclonal anti-DDDDK and incubated for 1 h at 37°C. The  
332 cells were washed and treated with 1000 fold diluted FITC conjugated goat anti-  
333 mouse IgG (Jackson ImmunoResearch lab., Baltimore, Maryland, USA) and  
334 incubated for 1 h at 37°C. The cells were washed once respectively, fixed using 2%  
335 (v/v) formaldehyde and viewed under CLSM with Plan-apochromat 100 × oil lens  
336 and 20 ×, respectively. Zen LE software available on Carl Zeiss website was used for  
337 image analysis.

### 338 Large Spheroids Preparation and VLP-rscFv-SRB Delivery

339 Large spheroids mold of 0.8 mm × 0.8 mm (diameter × depth) with 5 × 7 array using  
340 3D Petri dish (MicroTissues Inc., Rhodes Island, USA) were used to produce 500 μm  
341 diameter spheroids as per kit protocol. LS174T cells resuspended in 200 μL growth  
342 medium ( $1.4 \times 10^5$  cells) were applied to equilibrated spheroid molds kept in 60 mm  
343 cell view cell culture plates (Greiner Bio-one GmbH, Maybachstr. 2, Germany) and  
344 incubated at 37°C in CO<sub>2</sub> incubator for 30 minutes resulting in large spheroid  
345 formation, confirmed with 2 × lens of Olympus SZX14 microscope (Olympus, Tokyo,  
346 Japan).

347 One hundred micrograms of VLP-rscFv-SRB mixture were added to spheroids  
348 and incubated at 37°C in CO<sub>2</sub> incubator for 3 h. The spheroids were then washed with  
349 growth medium and treated with 250 fold diluted mouse monoclonal anti-DDDDK in  
350 500 μL growth media and incubated at 37°C in CO<sub>2</sub> incubator for 1 h. The spheroids  
351 were washed with fresh growth medium and treated with 500 fold diluted goat anti-  
352 mouse IgG (H+L) conjugated with FITC (Jackson ImmunoResearch lab.) in 500 μL  
353 growth medium and incubated at 37°C in CO<sub>2</sub> incubator for 1 h. Finally the cells  
354 were washed with growth medium and observed under live condition using 10 ×

355 apochromat lens of CLSM. Z-stacking was performed for 338  $\mu\text{m}$  in-depth of  
356 spheroid with each cross-sectional scanned layer of 1  $\mu\text{m}$ . All the Z-stacked images  
357 collected were rendered to prepare the 3D model using Zen LE 2011 version software  
358 available on Carl Zeiss website.

## 359 **RESULTS**

### 360 **Expression and Purification of rscFvs and gag Proteins**

361 Expression of rscFvs (~32 kDa) and gag protein was confirmed in purified samples  
362 collected from silkworm larvae hemolymph co-injected with both BmNPV/RSV-gag-  
363 577 and BmNPV/rscFvs bacmids. The western blot data for gag confirmed with  
364 molecular weight as reported earlier (Fig. 1A) (4). The western blot data for rscFvs  
365 shows another 35 kDa band (Fig. 1B), the apparent increase by about 3 kDa results  
366 due to the cells inability to remove the Bombyxin signal sequence or the GPI anchor  
367 whose processing might be one of the reasons. Approximately 1.5 milligrams of  
368 purified VLP-rscFvs was isolated from 30 mL of silkworm larvae, and shows the  
369 presence of the rscFvs and gag bands in CBB stained SDS-PAGE gel (Fig. 1C).

### 370 **Confirmation of Antigenicity and GPI Anchorage**

371 The rscFvs specificity to bind to TAG-72 the marker on colon carcinoma is an  
372 important property. The antigen specificity of rscFvs was confirmed by ELISA using  
373 TAG-72 antigen. Compared to negative control without rscFvs, specificity of VLP-  
374 rscFvs for TAG-72 was 22 fold higher (Fig. 2A).

375         The GPI anchorage of rscFvs was investigated using PI-PLC treatment. PI-  
376 PLC treated wells compared to untreated wells showed around 40% decrease in signal

377 (Fig. 2B) indicating presence of GPI anchored scFv. VLPs only as negative control  
378 show no remarkable change.

### 379 TEM and ImmunoTEM Analysis of VLP-scFvs and VLP-rscFv-SRB

380 TEM images of purified VLPs-rscFvs show a distinctive bilayer that is usually  
381 present on enveloped VLPs with a diameter of 100 nm (Fig. 3A). The immuno-TEM  
382 images of VLP-rscFvs show presence of rscFvs particles on the surface of VLPs (Fig.  
383 3B). TEM images of purified LUVs packaged with SRB shows distinctive smooth  
384 shaped LUVs of approximately 100 nm in diameter (Fig. 3C). TEM images of VLP-  
385 rscFv-SRB associated with LUVs-SRB shows the lipid bilayer. The average size of  
386 VLP-rscFv-SRB from TEM images is around 120–150 nm in diameter (Fig. 3D).  
387 Immuno-TEM of VLP-rscFv-SRB shows presence of rscFvs particles on the surface  
388 of VLP-rscFv-SRB (Fig. 3E). VLP-rscFv-SRB TEM images show the association  
389 between VLP-rScFvs and LUV-SRB as shown by the arrows (Fig. 3F). Both VLP-  
390 rscFv-SRB and LUV-SRB have a high contrast but the distinctive bilayer of VLPs  
391 easily distinguishes the nanostructures and suggests that VLP-rscFvs can bind  
392 strongly to LUV-SRB at pH 7.5. The samples were passed through 200 nm  
393 nucleopore membrane to avoid aggregation among VLP-rscFvs before measuring size  
394 by DLS for quantitative analysis of size change. The peak of the number distribution  
395 for the diameter of LUV-SRB, VLP-rscFvs and VLP-rscFv-SRB from DLS data was  
396 around 68, 51, and 79 nm, respectively (Fig. 3G). The shift in diameter for VLP-  
397 rScFvs and VLP-rscFv-SRB from DLS was of 28 nm. The increase in diameter of  
398 VLP-rscFv-SRB might be due to association or fusion of LUV-SRB with VLP-rscFvs  
399 suggesting that VLP-rscFvs can bind strongly to LUV-SRB at pH 7.5. LUV-SRB  
400 association with VLP-rscFvs results due to presence of GP64 on VLP-rscFvs surface.

401           The result of hemolysis indicates that VLP-rscFvs-SRB associated with RBCs  
402 strongly to induce hemolysis at pH 7.5 (Fig. 4), suggesting that VLP-rscFvs can bind  
403 strongly LUV-SRB. The negative control using BSA showed zero percent hemolysis  
404 (Data not shown).

#### 405 Localization of VLP-rScFvs and VLP-rscFv-SRB

406 Purified VLP-rscFvs were viewed under CLSM, and 0.1–0.2  $\mu\text{m}$  big spots were  
407 observed after treatment with Alexa Fluor 594 conjugated anti-DDDDK (Fig. 5A–C),  
408 supporting that the presence of rscFvs in purified VLP-rscFvs as shown in the  
409 schematic representation (Fig. 5D). The purified VLP-rscFvs show specificity to the  
410 TAG-72 antigen present on LS174T cells surface (Fig. 6A–D). The rscFvs presence  
411 and its localization were confirmed in LS174T cells (Fig. 6C and D). As a negative  
412 control, LS174T cells were treated with VLPs without rscFvs and they show no  
413 fluorescence for the affinity tag of scFv (Fig. 6E–H). Purified VLP-rscFVs was added  
414 to HEK293 cells to further confirm the specific binding of the VLP-rscFvs  
415 irrespective of any influence from lipid layer around VLPs, shows only plasma  
416 membrane localizing dye and no fluorescence for rscFvs (Fig. 6I–L). Thus VLP-rscFv  
417 can bind to LS174T cells specifically via scFv for TAG-72 antigen.

#### 418 Association of VLP-rscFvs with SRB and Targeting the Cells and Spheroids

419 LS174T cells with and without VLP-rscFvs-SRB treatment confirmed the delivery of  
420 SRB to cells (Fig. 7A–F). Approximately 3  $\mu\text{g}$  of VLP-rscFvs-SRB treated cells show  
421 FITC fluorescence for the affinity tag of rscFvs and SRB, respectively (Fig. 7A and  
422 B). In negative control cells treated with LUV-SRB or 1mM SRB only showed  
423 insignificant fluorescence of FITC and SRB (Fig. 7D-E and Supplementary Fig. 3).

424 VLP-rscFvs-SRB binding to cancer cells is facilitated by rscFvs specificity for TAG-  
425 72, leading to the delivery of SRB the test model dye to cell (Supplementary Fig. 1).

426 Large spheroids of 500 micrometers in diameter were produced using 3D  
427 agarose scaffold ( $5 \times 7$  arrays) (Supplementary Fig. 2). The spheroids were spherical  
428 and there was no aggregation of cells on the scaffold body other than the intended  
429 area. Approximately 2.8  $\mu\text{g}$  of VLP-rscFv-SRB per spheroid was incubated and  
430 fluorescence of SRB and FITC channels was observed as shown schematically from  
431 bottom (Fig. 8A). All the images for Z-stacking of 1  $\mu\text{m}$  thickness were taken from  
432 the bottom to top. The rendered images showed SRB at a depth of 100–150  $\mu\text{m}$  from  
433 the bottom of spheroid (Fig. 8B). FITC denoting rScFvs was observed at a depth of  
434 about 150–250  $\mu\text{m}$  from the bottom of the spheroid (Fig. 8C). The depth indicator  
435 from the merged picture shows there is overlap between SRB and rScFvs respectively  
436 at 100–150 $\mu\text{m}$  from the bottom as observed by the yellow color due to mixing of red  
437 and green channel colors (Fig. 8D). SRB (Fig. 8B) fluorescence and scFvs signals  
438 (Fig. 8C) were overlapped on the surface of the spheroid, indicating that scFv-  
439 displaying VLP bound to the cells on the surface of LS174T spheroid and carried  
440 SRB to these cells.

## 441 DISCUSSION

442 Many kinds of drug delivery systems targeting tumors for therapy using liposome's  
443 and VLPs of different compositions and proteins are being developed for delivering  
444 genes or drugs to mammalian cells (16, 36, 37). Here the novel use of VLPs  
445 displaying rScFvs with SRB as a model dye was reported to confirm the hypothesis of  
446 using VLP-rscFvs as a new drug delivery system. In order to develop the delivery  
447 system an expression system using silkworm larvae was established and VLP-rscFvs

448 expression and purification in milligram levels was confirmed. rscFvs expression and  
449 its display on the VLPs was facilitated by bombyxin signal sequence from *Bombyx*  
450 *mori* added to N-Terminal side of rscFvs (5). The signal sequence facilitates the  
451 rscFvs to reach the plasma membrane where VLPs formation takes place and they are  
452 secreted into silkworm larval hemolymph. gag protein shows different bands due to  
453 protease activity present in silkworms hemolymph as shown before (4, 18, 23). gag  
454 (~42 kDa) protein can be confirmed by CBB staining but the other band intensities  
455 were low for detection by CBB staining.

456 Many reported approaches use scFvs conjugated to drugs or proteins, but  
457 bottleneck of efficient conjugation and the resulting loss of function is a leading cause  
458 for less use of scFvs for therapy (17). In the present study, the high specificity of  
459 rscFvs displayed on VLPs is directly related with proper folding as there is no loss of  
460 function. The current protein expression model expresses two or more proteins  
461 independent of each other and the assembly takes place on the plasma membrane  
462 independent of each other with no protein folding constraints due to fusion. Thus the  
463 assembled proteins retain their native structures and functions. gag protein self  
464 assembly is well documented, its well suited for forming VLPs and display of foreign  
465 proteins (1, 5). Use of GPI anchor to display protein embedded in VLPs lipid bilayer  
466 and retaining the high antigenicity at the same time has been reported previously (5).

467 In the present study, a novel strategy employing GPI anchored scFvs on  
468 macromolecular nano-structures is tried. GPI anchoring was confirmed by PI-PLC  
469 treatment, an enzyme specifically cleaving the phosphodiester bond anchoring the  
470 protein to fatty acid chains in lipid layer of VLPs. The high antigen specificity of  
471 rscFvs against TAG-72 showed that the displayed protein is properly folded with no  
472 loss in function due to anchoring. VLP-rscFvs and VLP-rscFv-SRB displaying rscFvs

473 was confirmed by TEM and the qualitative analysis of TEM images shows the size  
474 increase. To understand the size increase of VLP-rscFv and VLP-rscFv-SRB a  
475 quantitative analysis using DLS was done, which showed a spread out in size as the  
476 current, expression system produces VLPs of varying size displaying different  
477 number of proteins. The exact mechanism involved in the current method to produce  
478 VLP-rscFv-SRB is unclear leading to association of LUV-SRB with VLP-rscFv and  
479 further work is needed.

480           Small scFvs anchored using GPI on VLPs can serve as an important tool for  
481 targeting cancer markers and support a robust delivery system. Here we propose using  
482 VLP-rscFv-SRB a composite macromolecular nanostructure with SRB to be delivered  
483 to spheroids in vitro as a model. The shape of the VLPs-rscFvs was similar as that of  
484 the VLPs (25). During the assembly of the macromolecular nanostructure GP64 is  
485 also peppered on top of VLPs due to the use of BmNPV expression system in  
486 silkworms as reported before (25). The apparent increase in diameter of VLPs-rscFvs  
487 could be attributed to insertion of the rscFvs and GP64 protein molecules together in  
488 between the gag monomers when the macromolecular nanostructure assembly takes  
489 place. The mechanism and number of proteins inserted per VLPs is not clear and  
490 needs to be further investigated. But GP64 is a well-studied fusion protein that forms  
491 large pore and due to presence of GP64, VLP-rscFvs with relative ease could be  
492 associated with SRB using LUV-SRB at neutral pH. To support this hypothesis GP64  
493 function peppered on VLP-rscFvs was confirmed by hemolysis assay. The exact  
494 mechanism behind the association using LUV-SRB and VLP-rscFv needs to be  
495 further studied. rscFvs presence was confirmed on VLPs before and after fusion with  
496 LUVs-SRB. Association of dye did not influence presence of rscFvs opening the

497 prospect of displaying multiple proteins on top of VLPs to target various types of  
498 tumors in future.

499 Cancer cell based assay reported here uses the binding specificity of VLP-  
500 rscFvs to TAG-72 present on the cancer cells surface. As a negative control HEK293  
501 cells were used without any TAG-72 on its surface to show the binding specificity.  
502 The binding specificity to TAG-72 on cancer cell plasma membrane was confirmed  
503 by co-localization studies using membrane-localizing dye. VLP-rscFv-SRB functional  
504 property of binding was also confirmed in a similar manner with cancer cells, which  
505 confirmed association of LUV-SRB to VLP-rscFv, does not hinder in the binding  
506 specificity of rscFv. Here we propose a hypothesis wherein the rscFvs on VLP-rscFv-  
507 SRB bind with TAG-72 present on the cells leading to the delivery of the dye to cells  
508 (Supplementary Fig. 1). The presence of both SRB and rscFv co-localization takes  
509 place as observed by the merged yellow color resulting due to mixing of red and  
510 green color channels of the dye. Based on this hypothesis VLP-rscFv-SRB delivery of  
511 SRB to spheroids were confirmed by the co-localization of rscFvs and SRB. The  
512 presence of both SRB and rscFvs and its depth in the spheroids based on the rendered  
513 image generated using the z-stacked image is about 100–150  $\mu\text{m}$  within 3 h of the  
514 incubation period. SRB is well known for cancer cell cytotoxicity assay studies owing  
515 to its sensitivities but the primary motive here was to show the delivery of the dye to  
516 the spheroids. The endocytosis pathway and the penetration property of the  
517 fluorescent probe SRB needs to be further investigated. In the current research it was  
518 used as a model for confirming the delivery only.

## 519 **CONCLUSIONS**

520 This study shows two novel aspects, first is the novel use of GPI anchors successfully  
521 displaying rscFvs on top of VLPs. By placing rscFvs specific towards TAG-72  
522 displaying on top of the VLPs the biofunctional ability of VLPs as a composite  
523 macromolecular nanostructure were obtained to target tumors. In order to test this  
524 hypothesis VLP-rscFvs associated with LUV-SRB were used here as a test model to  
525 deliver to spheroids, a well-studied ex vivo tumor model. The second novel aspect of  
526 this study is the use of GP64 present on VLPs surface due to silkworm expression  
527 system for producing VLPs-rscFv-SRB at neutral pH. Thus efficient expression can  
528 be done using silkworm expression system and the purified VLP-rscFvs can be  
529 associated with dyes in a simple way facilitated by GP64. In future other known drugs  
530 for colon carcinoma can be tried using similar principle.

## 531 **ACKNOWLEDGEMENTS**

532 We thank Professor Hiroshi Ueda (Tokyo Institute of Technology, Japan) for the kind  
533 gift of plasmid carrying ScFv cDNA. This work was supported partly by Grant-in-Aid  
534 for Scientific Research (A) Grant No.22248009 and partly by Promotion of Nanobio-  
535 Technology Research to support Aging and Welfare Society from the Ministry of  
536 Education, Culture, Sports, Science and Technology, Japan. There was no additional  
537 external funding received for this study.

## 538 **REFERENCES**

- 539 1. Deo VK, Tsuji Y, Yasuda T, Kato T, Sakamoto N, Suzuki H, Park EY.  
540 Expression of an RSV-gag virus-like particle in insect cell lines and silkworm  
541 larvae. *J Virol Methods*. 2011;177:147-152.
- 542 2. Medina G, Pincetic A, Ehrlich LS, Zhang Y, Tang Y, Leis J, Carter CA. Tsg101  
543 can replace Nedd4 function in ASV Gag release but not membrane targeting.  
544 *Virology*. 2008;377:30-38.

- 545 3. Waheed AA, Freed EO. The Role of Lipids in Retrovirus Replication. *Viruses*.  
546 2010;2:1146-1180.
- 547 4. Ma YM, Vogt VM. Rous sarcoma virus Gag protein-oligonucleotide interaction  
548 suggests a critical role for protein dimer formation in assembly. *J Virol*.  
549 2002;76:5452-5462.
- 550 5. Deo V, Yoshimatsu K, Otsuki T, Dong J, Kato T, Park EY. Display of *Neospora*  
551 *caninum* surface protein related sequence 2 on Rous sarcoma virus-derived gag  
552 protein virus-like particles. *J Biotechnol*. 2013;165:69-75.
- 553 6. Fankhauser N, Maser P. Identification of GPI anchor attachment signals by a  
554 Kohonen self-organizing map. *Bioinformatics*. 2005;21:1846-52.
- 555 7. Pierleoni A, Martelli PL, Casadio R. PredGPI: a GPI-anchor predictor. *BMC*  
556 *Bioinformatics*. 2008;9:392-402.
- 557 8. Hessa T, Meindl-Beinker NM, Bernsel A, Kim H, Sato Y, Lerch-Bader M,  
558 Nilsson I, White SH, von Heijne G. Molecular code for transmembrane-helix  
559 recognition by the Sec61 translocon. *Nature*. 2007;450:1026-1030.
- 560 9. Butikofer P, Malherbe T, Boschung M, Roditi I. GPI-anchored proteins: now you  
561 see 'em, now you don't. *Faseb J*. 2001;15:545-548.
- 562 10. Derdak SV, Kueng HJ, Leb VM, Neunkirchner A, Schmetterer KG, Bielek E,  
563 Majdic O, Knapp W, Seed B, Pickl WF. Direct stimulation of T lymphocytes by  
564 immunosomes: virus-like particles decorated with T cell receptor/CD3 ligands  
565 plus costimulatory molecules. *Proc Natl Acad Sci USA*. 2006;103:13144-13149.
- 566 11. Dangaj D, Abbott KL, Mookerjee A, Zhao A, Kirby PS, Sandaltzopoulos R,  
567 Powell DJ, Lamaziere A, Siegel DL, Wolf C, Scholler N. Mannose receptor  
568 (MR) engagement by mesothelin GPI anchor polarizes tumor-associated  
569 macrophages and is blocked by anti-MR human recombinant antibody. *PLoS One*.  
570 2011;6:28386-99.
- 571 12. Wen M, Arora R, Wang H, Liu L, Kimata JT, Zhou P. GPI-anchored single chain  
572 Fv-an effective way to capture transiently-exposed neutralization epitopes on  
573 HIV-1 envelope spike. *Retrovirol*. 2010;7:79-96.
- 574 13. Chames P, Baty D. Bispecific antibodies for cancer therapy. *Curr Opin Drug*  
575 *Discov Devel*. 2009;12:276-283.
- 576 14. P. Chames, M. Van Regenmortel, E. Weiss, D. Baty. Therapeutic antibodies:  
577 successes, limitations and hopes for the future. *Br J Pharmacol*. 2009;157:220-33.
- 578 15. Alderson RF, Toki BE, Roberge M, Geng W, Basler J, Chin R, Liu A, Ueda R,  
579 Hodges D, Escandon E, Chen T, Kanavarioti T, Babe L, Senter PD, Fox JA,  
580 Schellenberger V. Characterization of a CC49-based single-chain fragment-beta-  
581 lactamase fusion protein for antibody-directed enzyme prodrug therapy (ADEPT).  
582 *Bioconjug Chem*. 2006;17:410-418.
- 583 16. Arruebo M, Vilaboa N, Sáez-Gutierrez B, Lamba J, Tres A, Valladares M,  
584 González-Fernández Á. Assessment of the Evolution of Cancer Treatment  
585 Therapies. *Cancers*. 2011;3:3279-3330.
- 586 17. Chames P, Van RM, Weiss E, Baty D. Therapeutic antibodies: successes,  
587 limitations and hopes for the future. *Br J Pharmacol*. 2009;157:220-33.
- 588 18. Pavlinkova G, Beresford GW, Booth BJ, Batra SK, Colcher D. Pharmacokinetics  
589 and biodistribution of engineered single-chain antibody constructs of MAb CC49  
590 in colon carcinoma xenografts. *J Nucl Med*. 1999;40:1536-1546.
- 591 19. Iyer U, Kadambi V. Antibody drug conjugates - Trojan horses in the war on  
592 cancer. *J Pharmacol Toxicol Methods*. 2011;64:207-212.

- 593 20. Monsma SA, Blissard GW. Identification of a membrane fusion domain and an  
594 oligomerization domain in the baculovirus GP64 envelope fusion protein. *J Virol.*  
595 1995;69:2583-95.
- 596 21. Monsma SA, Oomens AG, Blissard GW. The GP64 envelope fusion protein is an  
597 essential baculovirus protein required for cell-to-cell transmission of infection. *J*  
598 *Virol.* 1996;70:4607-16.
- 599 22. Oomens AG, Monsma SA, Blissard GW. The baculovirus GP64 envelope fusion  
600 protein: synthesis, oligomerization, and processing. *Virol.* 1995;209:592-603.
- 601 23. Li Z, Blissard G. *Autographa californica* multiple nucleopolyhedrovirus GP64  
602 protein: roles of histidine residues in triggering membrane fusion and fusion pore  
603 expansion. *J Virol.* 2011;85:12492-12504.
- 604 24. Kamiya K, Tsumoto K, Arakawa S, Shimizu S, Morita I, Yoshimura T, Akiyoshi  
605 K. Preparation of connexin43-integrated giant Liposomes by a baculovirus  
606 expression-liposome fusion method. *Biotechnol Bioeng.* 2010;107:836-843.
- 607 25. Tsuji Y, Deo VK, Kato T, Park EY. Production of Rous sarcoma virus-like  
608 particles displaying human transmembrane protein in silkworm larvae and its  
609 application to ligand-receptor binding assay. *J Biotechnol.* 2011;155:185-92.
- 610 26. Ong SM, Zhao Z, Arooz T, Zhao D, Zhang S, Du T, Wasser M, van-Noort D, Yu  
611 H. Engineering a scaffold-free 3D tumor model for in vitro drug penetration  
612 studies. *Biomaterials.* 2010;31:1180-1190.
- 613 27. Jiang X, Sha X, Xin H, Xu X, Gu J, Xia W, Chen S, Xie Y, Chen L, Chen Y,  
614 Fang X. Integrin-facilitated transcytosis for enhanced penetration of advanced  
615 gliomas by poly(trimethylene carbonate)-based nanoparticles encapsulating  
616 paclitaxel. *Biomaterials.* 2013;34:2969-2979.
- 617 28. Jiang X, Xin H, Gu J, Xu X, Xia W, Chen S, Xie Y, Chen L, Chen Y, Sha X,  
618 Fang X. Solid tumor penetration by integrin-mediated pegylated  
619 poly(trimethylene carbonate) nanoparticles loaded with paclitaxel. *Biomaterials.*  
620 2013;34:1739-1746.
- 621 29. Kamiya K, Kobayashi J, Yoshimura T, Tsumoto K. Confocal microscopic  
622 observation of fusion between baculovirus budded virus envelopes and single  
623 giant unilamellar vesicles. *Biochimica et Biophysica Acta.* 2010;1798:1625-1631.
- 624 30. Houghton P, Fang R, Techatanawat I, Steventon G, Hylands P, Lee C. The  
625 sulphorhodamine (SRB) assay and other approaches to testing plant extracts and  
626 derived compounds for activities related to reputed anticancer activity. *Methods*  
627 *(San Diego, Calif.).* 2007;42:377-387.
- 628 31. Pierleoni A, Martelli PL, Casadio R. PredGPI: a GPI-anchor predictor. *BMC*  
629 *Bioinformatics.* 2008;9:392.
- 630 32. Sanger F, Nicklen S, Coulson AR. DNA sequencing with chain-terminating  
631 inhibitors. *Proc Natl Acad Sci USA.* 1977;74:5463-5467.
- 632 33. Deo VK, Hiyoshi M, Park EY. Construction of hybrid *Autographa californica*  
633 nuclear polyhedrosis bacmid by modification of p143 helicase. *J Virol Methods.*  
634 2006;134:212-216.
- 635 34. Maeda T, Ohnishi S. Activation of influenza virus by acidic media causes  
636 hemolysis and fusion of erythrocytes. *FEBS Lett.* 1980;122:283-7.
- 637 35. Tamba Y, Yamazaki M. Single giant unilamellar vesicle method reveals effect of  
638 antimicrobial peptide magainin 2 on membrane permeability. *Biochem.*  
639 2005;44:15823-33.
- 640 36. Bolhassani A, Safaiyan S, Rafati S. Improvement of different vaccine delivery  
641 systems for cancer therapy. *Mol Cancer.* 2011;10:3.

- 642 37. Keswani R, Pozdol I, Pack D. Design of Hybrid Lipid/Retroviral-Like Particle  
643 Gene Delivery Vectors. Mol Pharmaceut. 2013;10:1725-35.  
644

## 645 **FIGURE LEGENDS**

646 **Fig. 1.** Western blotting of purified samples of VLP-rscFvs. gag-577 (A) and  
647 rscFvs (B) were detected by western blotting using rabbit anti-gag primary  
648 antibody and mouse anti-DDDDK primary antibody, respectively. Secondary  
649 antibodies used for detection of gag-577 (A) and rScFvs (B) were goat anti-  
650 rabbit IgG and goat anti-mouse IgG, respectively. Lane 1: molecular weight  
651 marker; lane 2: 1  $\mu$ g of VLP-rscFvs samples. (C) CBB stained 10% SDS-  
652 PAGE gel of VLP-rscFvs samples. Lane 1: molecular weight marker, lanes 2  
653 and 3: 1  $\mu$ g and 5  $\mu$ g of VLP-rscFvs samples, respectively. The black and  
654 white arrows show the rscFvs and gag (some minor cleaved bands of gag are  
655 also observed between 40~61 kDa), respectively.

656 **Fig. 2.** (A) Confirmation of antigenicity was tested using 20 U of TAG-72 per  
657 well. Five micrograms per well of purified VLP-rscFvs protein samples were  
658 loaded and the wells were probed with mouse anti-DDDDK and secondary  
659 antibodies were goat anti-mouse IgG for rscFvs. Black and white bars denote  
660 VLP-rscFvs and VLPs samples, respectively. Data are the mean $\pm$ SD ( $n=3$ )  
661 (B) Presence of GPI anchor was confirmed by PI-PLC treatment by ELISA  
662 method. Black and white bars represent with and without PI-PLC wells. Data  
663 are the mean $\pm$ SD ( $n=3$ ).

664 **Fig. 3.** TEM and Immuno-TEM pictures. (A) VLP-rscFvs. Scale bar is 200 nm.  
665 (B) VLP-rscFvs with 10 nm gold particles. Scale bar is 100 nm. (C) LUV-SRB.  
666 Scale bar is 100 nm. (D) VLP-rscFv-SRB. Scale bar is 200 nm. (E) VLP-  
667 rscFv-SRB with 10 nm gold particles. Scale bar is 200 nm. (F) VLP-rscFv-

668 SRB showing association. Scale bar is 100 nm. Black arrows denote  
669 distinctive bilayer of VLPs. White arrows indicate LUVs-SRB. (G) DLS data of  
670 LUV-SRB (long dash line), VLP-rscFvs (solid line) and VLP-rscFv-SRB (short  
671 dash line). One hundred micrograms of VLP-rscFvs and VLP-rscFv-SRB  
672 were used for assay, showing the shift in size (diameters in nm) before and  
673 after association.

674 **Fig. 4.** Purified VLP-rscFv was used to qualitatively evaluate GP64 functions  
675 by hemolysis assay. Rabbit erythrocytes when come in contact with GP64 a  
676 pore forming protein causes an increase in porosity of the membrane leading  
677 to leakage of heme into supernatant, which is measured colorimetrically.

678 **Fig. 5.** VLPs-rscFvs were observed by CLSM after treatment with Alexa594  
679 conjugated anti-DDDDK (A), in bright field image (B) and the merged image  
680 (C). Scale bar is 1  $\mu$ m. (D) Schematic representation of VLP-rscFvs on the  
681 glass slide.

682 **Fig. 6.** CLSM pictures of LS174T cells with VLP-rscFvs (A-D), with VLPs (E-  
683 H), and HEK293T cells with VLP-rscFvs (I-L), respectively. (A, E, and I) DAPI  
684 and bright field overlapped image. (B, F, and J) BODIPY FL-C5-ceramide  
685 complexed to BSA for plasma membrane localization. (C, G, and K) Alexa594  
686 conjugated anti-DDDDK for rscFvs. (D, H, and L) Merged images of all the  
687 color channels. Scale bars denote 20  $\mu$ m.

688 **Fig. 7.** CLSM pictures of LS174T cells with (A-C) and without (D-F) VLP-  
689 rscFv-SRB treated for co-localization studies. (A and D) FITC-conjugated goat  
690 anti-mouse IgG against mouse anti-DDDDK image. (B and E) SRB image and

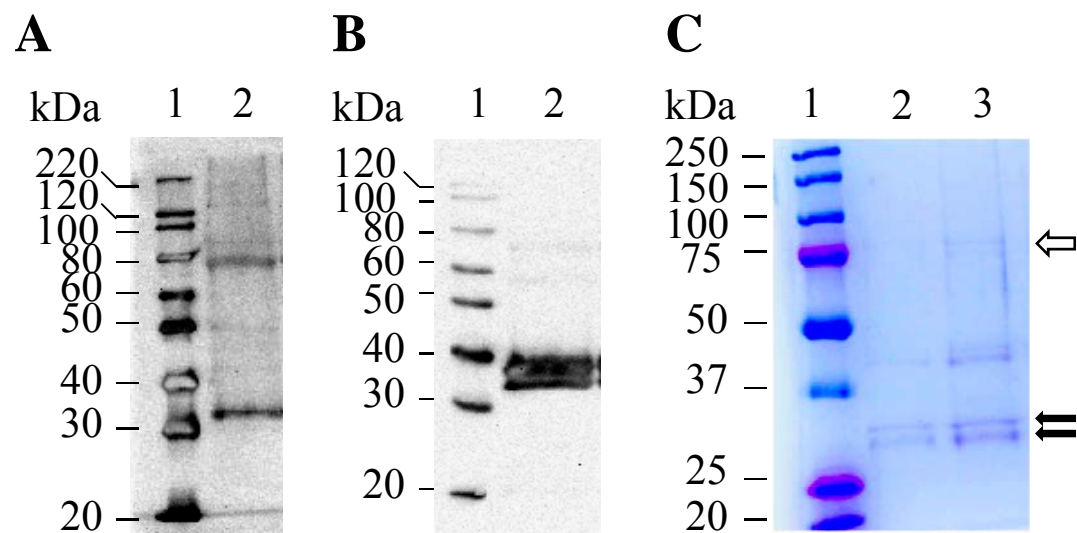
691 (C and F) bright field plus merged images of all the color channels. Scale bars  
692 denote 5  $\mu\text{m}$ .

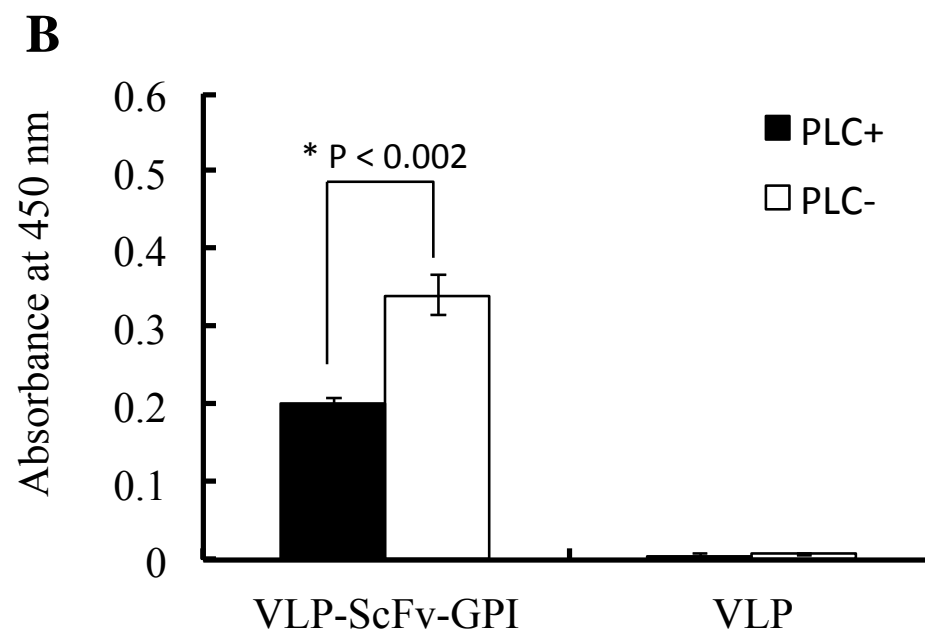
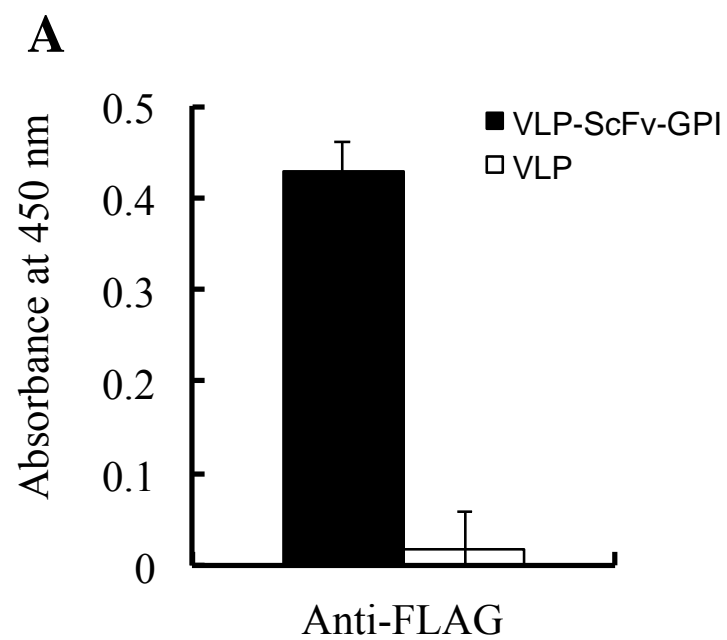
693 **Fig. 8.** The rendered color-coded depth projection of the entire z-stack of x-y  
694 images (n=338) for the spheroid. (A) The schematic representation to show  
695 the lens position and the Z-stacking position. (B) Color coded depth projection  
696 of SRB. (C) Color coded depth projection of rscFvs. (D) Merged image of (B)  
697 and (C).

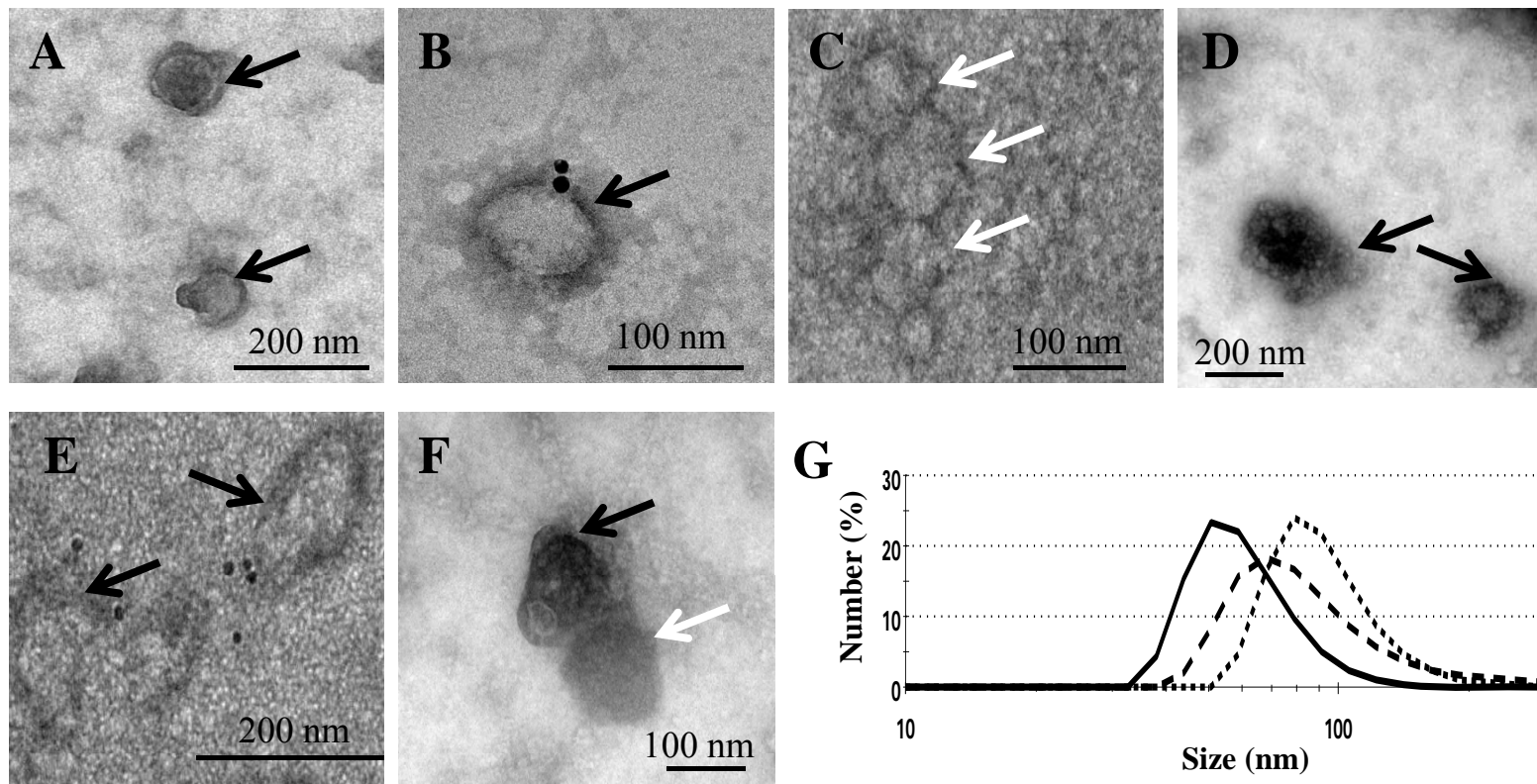
698 **Supplementary Fig. 1.** Schematic representation of the hypothesis behind  
699 the VLP-rscFv-SRB homing onto the cancer cells and delivery of dye to cells.

700 **Supplementary Fig. 2.** Large spheroids of 500  $\mu\text{m}$  diameter with  $5 \times 7$  array  
701 using 3D Petri dish were prepared. Scale bars are 500 $\mu\text{m}$ .

702 **Supplementary Fig. 3.** CLSM pictures of LS174T cells with DAPI plus bright  
703 field (A), 1 mM SRB (B) and merged images (C) of the color channels. Scale  
704 bars are 20  $\mu\text{m}$ .







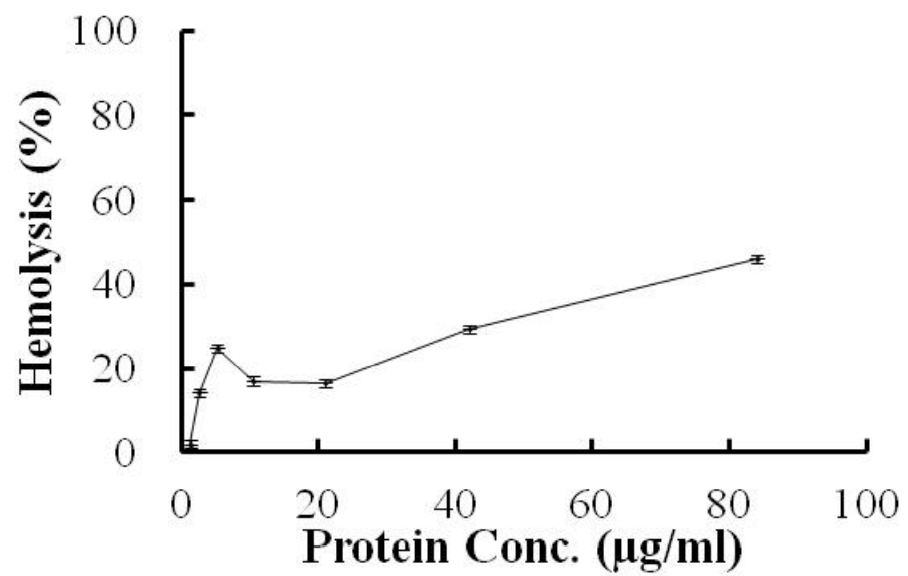
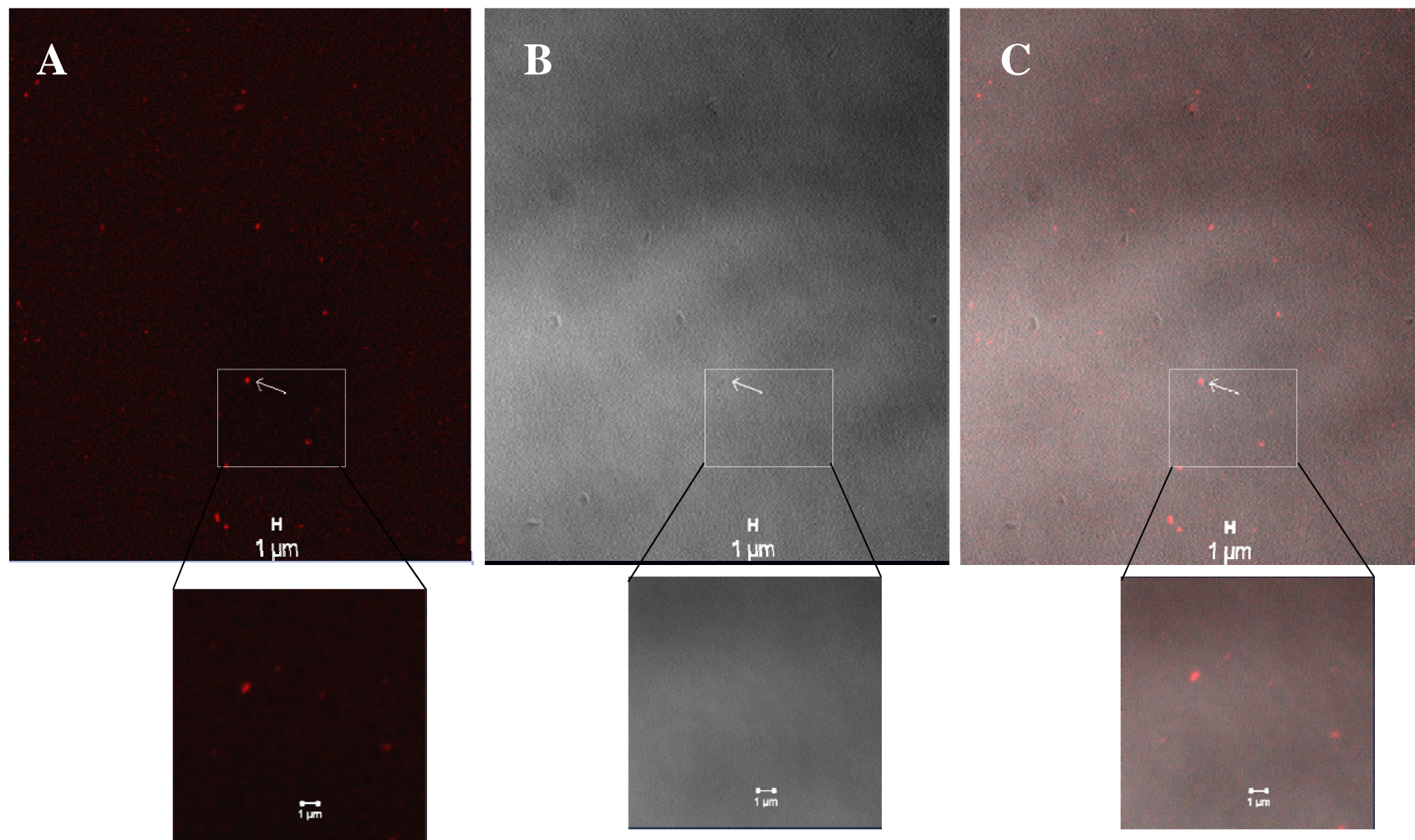
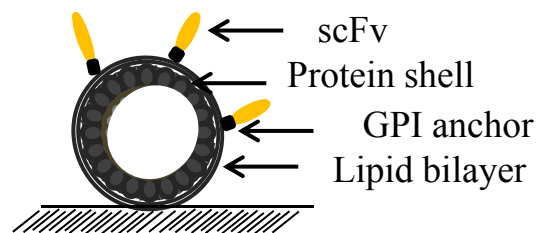
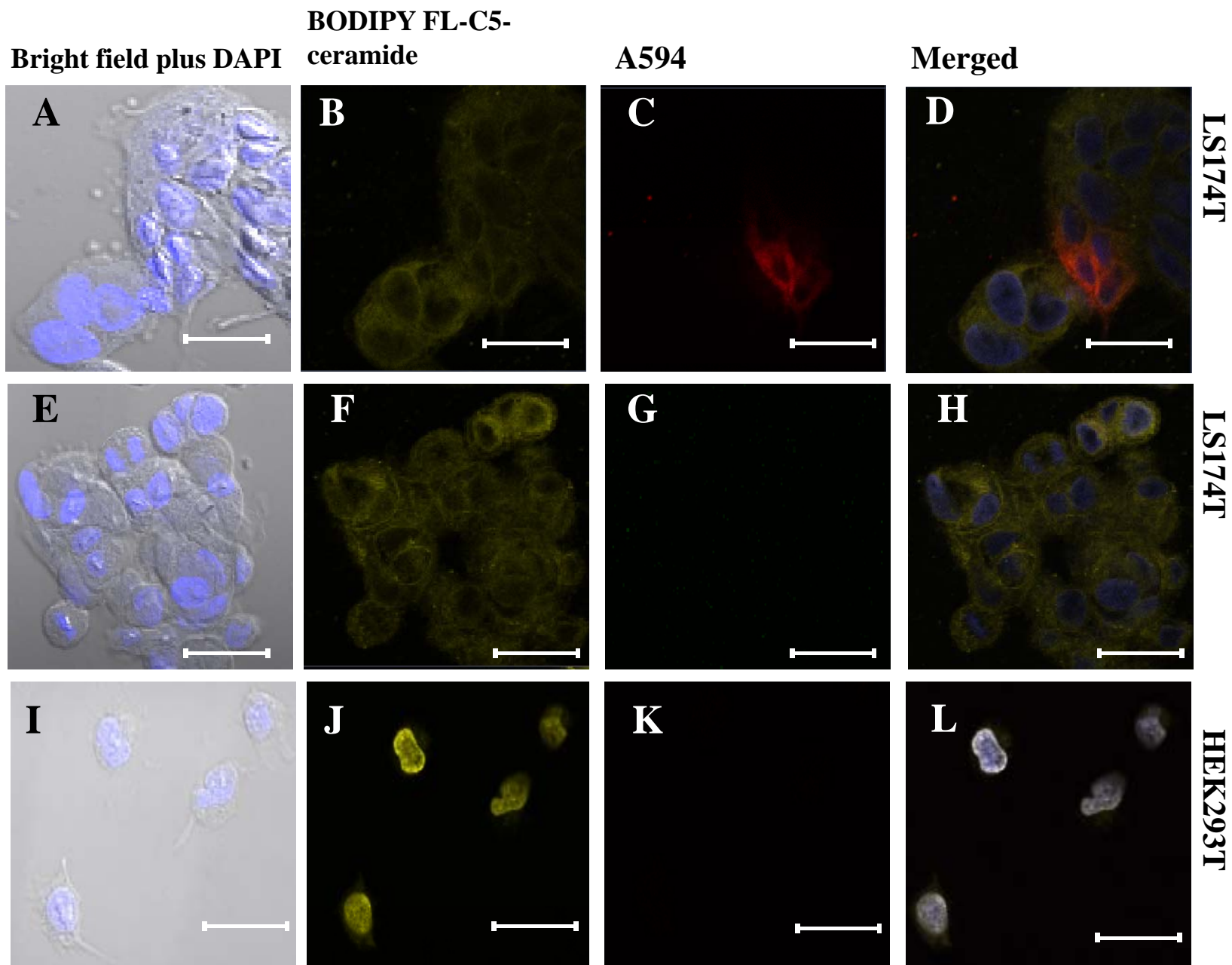


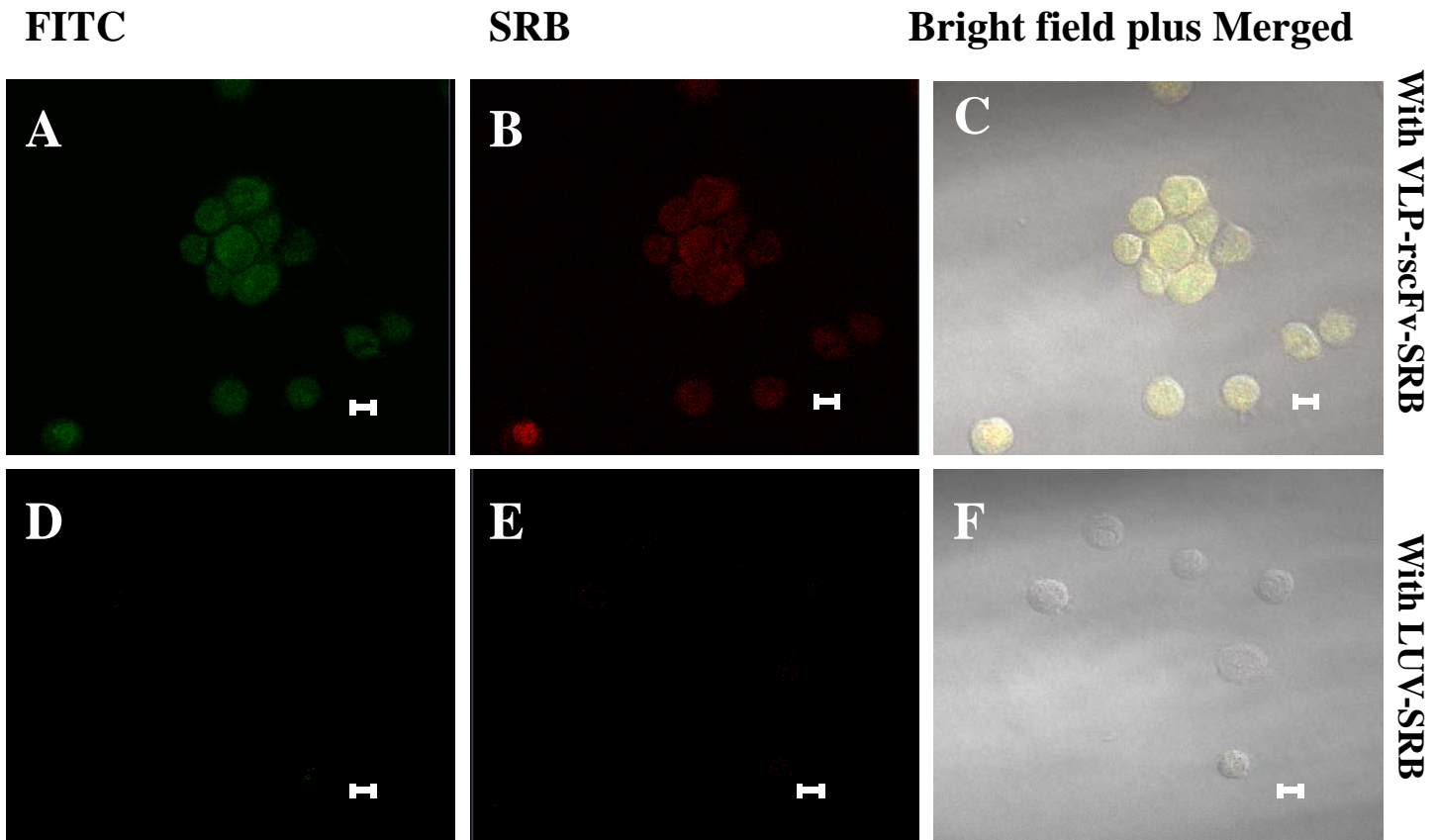
Fig. 5, Deo et al



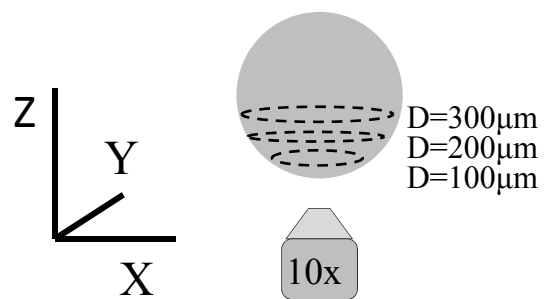
**D**



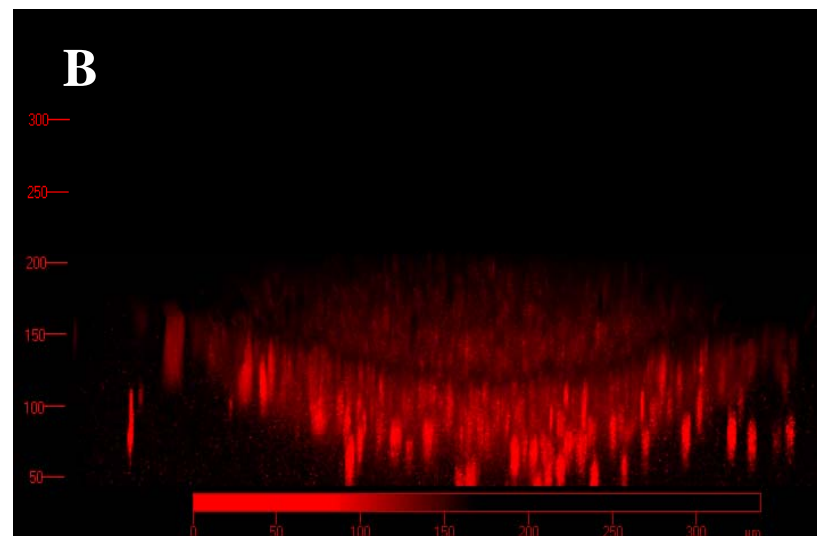




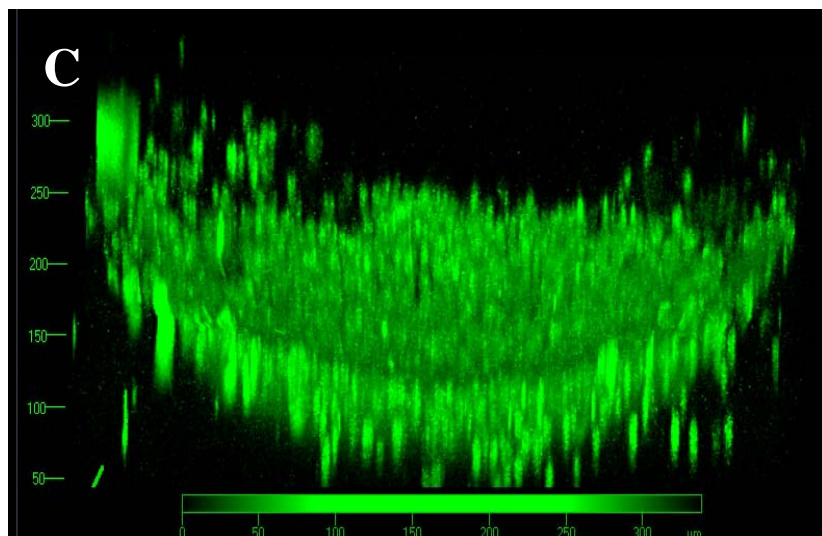
**A**



**B**



**C**



**D**

